Heat transport in three-layer turbulent thermal convection

Xiao-Zheng Zhao [1,2] Can Qiu,[2] Sheng-Qi Zhou [3,2] Yi-Zhen Li [4]
Heng-Dong Xi [5,2] and Ke-Qing Xia [1,6,2,*]

[1]*Department of Mechanics and Aerospace Engineering, Southern University of Science and Technology,*
Shenzhen 518055, China
[2]*Department of Physics, The Chinese University of Hong Kong, Shatin, Hong Kong, China*
[3]*State Key Laboratory of Tropical Oceanography, South China Sea Institute of Oceanology,*
Chinese Academy of Sciences, Guangzhou 510301, China
[4]*School of Aeronautics and Institute of Extreme Mechanics, Northwestern Polytechnical University,*
Xi'an 710072, China
[5]*School of Aeronautics and Institute of Extreme Mechanics and National Key Laboratory of Aircraft*
Configuration Design, Northwestern Polytechnical University, Xi'an 710072, China
[6]*Center for Complex Flows and Soft Matter Research, Southern University of Science and Technology,*
Shenzhen 518055, China

We report an experimental study of heat transport in a three-layer turbulent Rayleigh-Bénard convection. The experiments were conducted in a cylindrical cell (with diameter D) filled with a FC77 layer with height $H = D$. A very thin layer of water and a very thin layer of mercury were introduced to the top and bottom of the FC77 layer to provide slippery boundary conditions. We performed high spatial resolution temperature measurements across the water-FC77 and FC77-mercury interfaces, determined the temperatures at the two interfaces, the Rayleigh number (Ra) and the Nusselt number (Nu) across the FC77 layer. The experiments were conducted in the Ra range of 2.81×10^9 to 1.24×10^{11} for the FC77 layer. It is found that not only the amplitude but also the scaling exponent (with Ra) of Nu is greatly enhanced in this three-layer system compared to the canonical single-layer system, especially in the high Ra range. In particular, Nu first scales as $Ra^{0.31}$ and then $Ra^{0.38}$ when Ra exceeds a transitional Rayleigh number $Ra_t = 2.52 \times 10^{10}$, whereas in the canonical single-layer FC77 case, Nu is found to scale as $Ra^{0.26}$. Temperature measurements show that the boundary condition above and below the FC77 layer is asymmetric especially when $Ra > Ra_t$: the temperature drop across the top half (in contact with the water layer) of the FC77 layer is smaller than that across the bottom half (in contact with the mercury layer), and the top thermal boundary layer (TBL) becomes thinner and follows a steeper scaling with Ra compared to the bottom TBL. We consider a hypothetical experiment where the top and the bottom boundary conditions are symmetric, denoted as a "water-FC77-water" three-layer system, in which the temperature drop across the bottom boundary layer ΔT_b would be the same as that across the top boundary layer ΔT_t. We found in this water-FC77-water three-layer system, with the increase of Ra, Nu vs Ra scaling transitions from $Nu \sim Ra^{0.31}$ to $Nu \sim Ra^{0.46}$ with the transitional Ra the same as Ra_t identified before. A closer check of the evolution of Ra of the water layer, FC77 layer, and the mercury layer reveal that the transition of the Nu vs Ra scaling is due to the transition of the thin water layer from a conduction state to a convection state, whereas the mercury layer remains in a conduction state.

*Contact author: xiakq@sustech.edu.cn

I. INTRODUCTION

Thermal convection is a ubiquitous phenomenon in nature and in industrial applications. An idealized paradigm to study the ubiquitous convection phenomenon is the Rayleigh-Bénard convection (RBC) [1–3], which consists of a fluid layer confined between two parallel thermal conducting plates heated from below and cooled from above. The dynamics of the flow are determined by three dimensionless parameters: the Rayleigh number [$Ra = \alpha g H^3 \Delta T/(\nu \kappa)$] describing the intensity of buoyancy-driven turbulence, the Prandtl number ($Pr = \nu/\kappa$) characterizing the fluid properties, and the aspect ratio ($\Gamma = D/H$) representing the geometry of the convection cell. Here, g is the gravitational acceleration; α, ν, and κ denote the thermal expansion coefficient, kinematic viscosity, and thermal diffusivity of the working fluid, respectively, while ΔT is the temperature difference across the cylindrical convection cell with a diameter of D and height of H. The two response parameters are, respectively, the Nusselt number [$Nu = J/(\lambda \Delta T/H)$] ($\lambda$ is the thermal conductivity of the fluid), which characterizes the heat transport efficiency of the system; and the Reynolds number ($Re = uH/\nu$), which reflects the flow strength, where J is the total heat flux supplied to the convection cell and u is the characteristic velocity of the flow.

One of the central issues in the turbulent RBC is to understand how turbulent flow transports heat across the convective fluid layer. Numerous previous studies have attempted to modulate turbulent heat transport efficiency by modulating the plumes and the large-scale circulation, which are the main carriers of heat transfer. Typical modulation methods include tilting the system to change the large-scale flow structure [4–8] and adding geometric constraints to change the coherence of the flow structure [9–13]. Since the heat transport efficiency in the RBC is mainly limited by the boundary layer located near the hot and cold plates, these modulation methods do not break through the constraints of the boundary layer on the heat transport, so the improvement of the heat transport efficiency is relatively limited [1]. Therefore another common approach is to modulate the heat transport by modulating the interaction between the boundary layer and the bulk region, for example, by using rough elements as boundaries [14–19], bringing bubbles and particles into the system [20–23], introducing shear boundary conditions [24–28], adding oscillations [29–31], and so on.

The presence of a slip boundary can also significantly modulate the heat transport efficiency of the system compared to the canonical no-slip solid wall boundary condition. For example, Huang *et al.* through numerical simulation, recently found that the heat transport efficiency increases with the slip length [32]. However, there is a lack of systematic experimental studies on how heat transport efficiency changes when the boundary conditions deviate from the conventional no-slip boundary condition. Experimentally, slip boundary conditions are mainly achieved by mutually immiscible fluids with different densities. Previous studies on layered thermal convection have focused on the nonturbulent regime near the onset of convection [33–37], mainly describing the dependence of the coupling mode on the control parameters and the fluid properties. Recent studies have gradually moved to the turbulent regime; for example, Solomon and Gollub [38,39] experimentally revealed the dependence of heat transfer on the strength of the shear, which is induced by an immiscible mercury layer. Xie and Xia [40] experimentally explored the interplay between the flow dynamics behaviors of a two-layer flow and illustrated the dependence of the turbulent heat transport efficiency on the coupling modes of the two-layer fluid flow. Yoshida *et al.* [41,42] systematically modeled the effect of the viscosity ratio of the two layers and found that the coupling gradually transitions from viscous to thermal coupling with the increase of the viscosity ratio. Later, Noto *et al.* [43] determined the coupling structure between the two-layer fluids by developing a simultaneous measurement of the velocity field of the two layers. Liu *et al.* [44,45] revealed the criteria for the breakup of a two-layer fluid interface through numerical simulations and further extended the Grossmann-Lohse theory from canonical single-layer convection to a two-layer one. Huang *et al.* [46] investigated the thermal boundary layer between two-layer fluid interfaces and found that the boundary layer on a liquid interface can still be well described by the boundary layer equations on a solid boundary, except that for a liquid interface, a slip length needs to be introduced
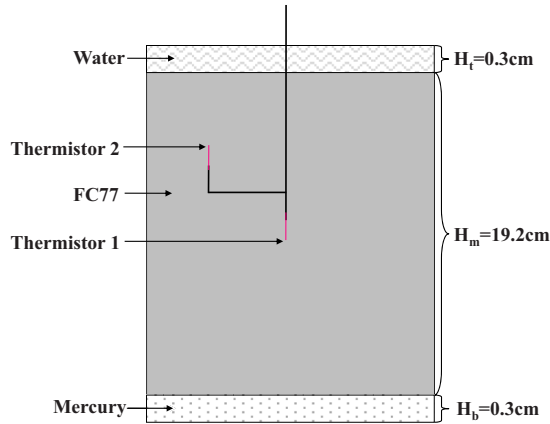
FIG. 1. The schematic of the convection cell, the three layers of fluids (from bottom to top, the three layers of mutually immiscible fluids are mercury, FC77, and water, and their heights are 0.3, 19.2, and 0.3 cm, respectively), and the thermistors.

into the boundary layer equations. Recently, Wang *et al.* explored heat transfer and flow structure in two-layer convection, and it is found that the global heat transfer can be divided into three regimes due to the evolution of the flow structure in the bottom layer, though the Prandtl number of each fluid layer was not constant during the experiment [47]. However, these studies in turbulent regimes have either focused on the effect of slip boundary on heat transport or on the turbulent structure of two-layer thermal convection. It is still unknown how heat transport evolves when both the top and the bottom boundary conditions are replaced with slip boundaries.

In this paper, we fill this gap by measuring the heat transport in a three-layer turbulent RBC with three immiscible fluids: mercury, FC77 (a type of Fluorinert electronic liquid from 3M company), and water. The middle thick FC77 layer is the main working fluid, while both the bottom thin mercury layer and the top thin water layer presumably provide slippery boundary conditions. Therefore, it is expected that the thermal boundary layers of the FC77 layer are modified and its heat transport behavior is altered. The remainder of this paper is organized as follows. The experimental setup is introduced in Sec. II. Section III presents the main experimental results, including the temperature drop across the two liquid-liquid interfaces, the Ra dependence of the heat transport, and the thermal boundary layer thickness of the middle FC77 layer. The main findings are summarized in Sec. IV.

II. EXPERIMENTAL SETUP

The convection cell used in the experiments has been described in detail previously [48,49], and only its key features are presented here. The top and the bottom plates of the convection cell are made of copper with thickness 1.4 cm and the sidewall is made of Plexiglas with thickness 0.3 cm. As shown in Fig. 1, the vertical cylindrical sidewall has a height of 19.8 cm and an inner diameter of 19.2 cm. The cell is filled with three mutually immiscible layers of fluids; they are, from bottom to top, mercury, FC77, and deionized water. The heights of these three layers are 0.3, 19.2, and 0.3 cm, respectively, so that the aspect ratio of the FC77 layer is $\Gamma = 1$. For convenience, the water, FC77, and mercury layers are referred to as the top, middle, and bottom layers, respectively. The middle FC77 layer is the main working fluid, while the top water layer and bottom mercury layers provide slip (or partially slip) boundary conditions. The physical properties of the three types of fluids at $30\,^\circ$C are listed in Table I for reference. The surface of the copper plate is coated with nickel to prevent oxidization and provide a mirror-finish surface. The nickel film is especially necessary because the copper plate easily reacts with mercury to form copper-mercury amalgams.

TABLE I. Physical properties of water, FC77, and mercury at 30 °C.

Fluids	ρ (kg/m^3)	λ (W/m K)	C_p (J/kg K)	α (1/K)	κ (m^2/s)	ν (m^2/s)
Water	996	0.614	4179	3.03×10^{-4}	1.48×10^{-7}	8.01×10^{-7}
FC77	1764	0.0626	1060	1.39×10^{-3}	3.34×10^{-8}	6.64×10^{-7}
Mercury	13477	8.26	140	1.81×10^{-4}	4.38×10^{-6}	1.12×10^{-7}

Five large thermistors with diameter 2.4 mm (model 44031, Omega Inc.) are embedded into the top (bottom) plate to measure the temperature in the plate, and they are 1 cm (0.4 cm) away from the fluid-solid interface for the top (bottom) plate. One of the five thermistors is located at the center of the plate, while the other four are evenly embedded at half the radius from the center. A different type of small thermistors with diameter 0.2 mm (model AB6E3-B05103J, Thermometrics Inc.) are used to measure the temperature in fluids. This thermistor has a response time of 15 ms, which ensures a high sensitivity to the temperature fluctuations. As shown in Fig. 1, two small thermistors are mounted on a frame made from a stainless-steel tube with diameter 1 mm. One of the thermistors (referred to as thermistor 1) is placed along the central line of the cell, which is used to measure the temperature across the mercury-FC77 interface. The other one (referred to as thermistor 2) for measuring the temperature across the FC77-water interface is at a half-radius away from the center line of the cell to avoid the influence of the filling stem which is at the center of the top plate. A motorized translation stage (MTS50, Thorlabs Inc.) is used to move the frame vertically with spatial resolution of 1 μm.

In order to have high precision heat transport measurements, the convection cell and the top plate are surrounded by two layers of nitrile rubber sheets and one layer of styrofoam for thermal insulation. The bottom plate lies in a copper basin with three wood plates in between. The temperature of the copper basin is regulated to be close to that of the bottom plate to minimize the heat exchange between the bottom plate and the surroundings. Finally, the whole apparatus was placed inside a homemade thermostat where the temperature was modulated to match the bulk temperature of the FC77 layer. The temporal and spatial temperature stability of the thermostat was better than 0.1 °C. During the experiment, the bulk temperature of the FC77 layer has been kept at around 31.6 °C, which corresponds to the Prandtl number Pr = 19.4. The bottom plate is heated by a heater embedded in the bottom plate, and the temperature of the top plate is regulated by a recirculating refrigerator (Polyscience 9702). The Rayleigh number Ra of the FC77 layer varies from 2.81×10^9 to 1.24×10^{11}.

III. RESULTS AND DISCUSSIONS

A. Temperature profiles across the interfaces

The main working fluid FC77 lies in between the thin mercury and water layers. To evaluate the heat transfer in the FC77 layer it is necessary to determine the temperatures at the mercury-FC77 interface and the FC77-water interface. To this end, we first make the measurement of the temperature across both the mercury-FC77 and the FC77-water interfaces. As shown in Fig. 1, the thermistors 1 and 2 are used to measure the temperature profile across the two interfaces. To measure the temperature across the mercury-FC77 layer, the frame is first set at the position such that thermistor 1 touches the interface which is determined approximately by a traveling microscope. It is then moved up to the position such that thermistor 1 is in the FC77 layer and about 2 mm above the interface. This is the starting point for our measurement of the mercury-FC77 interface. We then move the thermistor 1 downwards along the vertical direction across the interface step by step; the step is 0.2 mm when the thermistor is far away from the interface, and is 0.05 mm when the thermistor is approaching the interface. At each position, the temperature recording time varies from 30 to 120 min depending on Ra and its distance to the interface; the recording time is longer
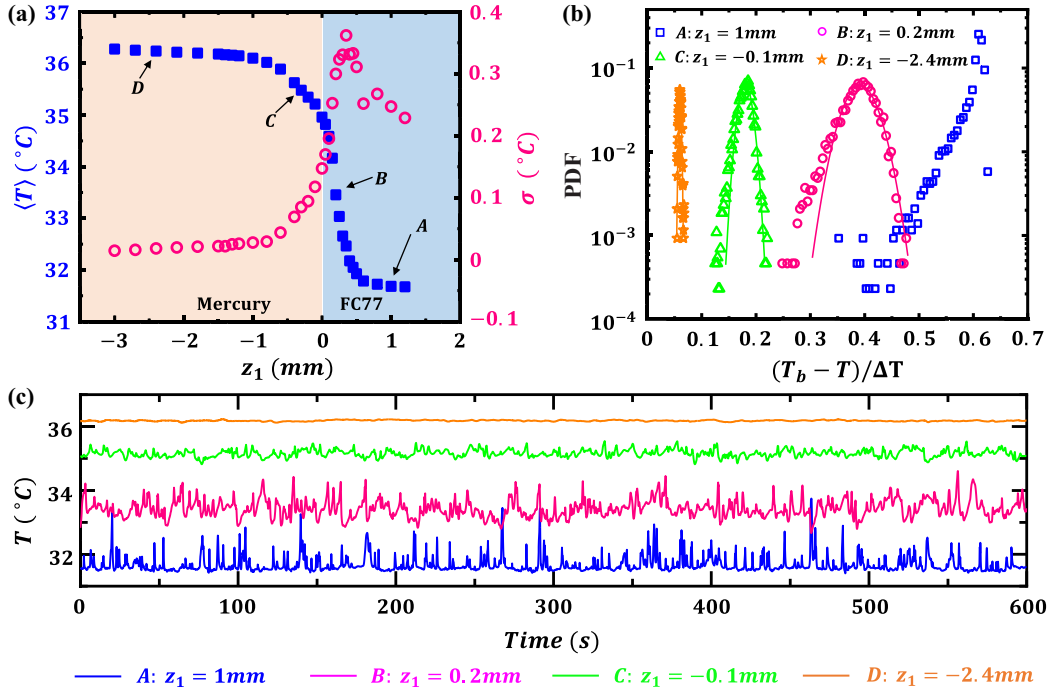
FIG. 2. (a) Mean temperature $\langle T \rangle$ and rms temperature σ profiles across the mercury and FC77 interface for Ra $= 3.85 \times 10^{10}$. Solid squares and open circles are $\langle T \rangle$ and σ respectively. (c) The time series and (b) the PDF of the temperatures at positions A, B, C, and D marked in (a). Please note that plotted in (b) is the PDF of $(T_b - T)/\Delta T$, not the temperature T itself, where T_b is the temperature of the bottom plate, and ΔT is the temperature difference across the FC77 layer. The curves in (b) are the Gaussian distribution function fits to the data.

when Ra is low or when the position is close to the interface. The z axis points upward, while the subscript 1 (2) of z denotes the measurement of the mercury-FC77 interface (FC77-water interface). A typical temperature profile consists of about 30 vertical positions across the interface.

Typical mean temperature $\langle T \rangle$ and rms temperature $\sigma = \langle (T - \langle T \rangle)^2 \rangle^{1/2}$ profiles across the mercury-FC77 interface for Ra $= 3.85 \times 10^{10}$ are shown in Fig. 2(a), where the heat flux provided to the bottom plate is 611.3 W/m^2 and the temperature on the top plate is 25.0 °C. As the thermistor is approaching the FC77-mercury interface from above (z_1 decreases), it can be seen from the figure that the mean temperature increases and can be roughly divided into several regions. The first region is the bulk region of the FC77 layer, where the mean temperature remains almost constant, as shown by the first three data points (from the right) shown in Fig. 2(a). With the decrease of z_1, the thermistor enters the second region where the mean temperature exhibits a significant increase. At the same time, the rms temperature increases to a maximum value and then decreases. The well-defined peak in the rms temperature profile indicates the beginning of the thermal boundary layer region of the FC77 layer. When the thermistor is about crossing the FC77-mercury interface, due to the existence of the surface tension, the interface is deformed, and forms a bump pointing to the mercury side. When the thermistor enters the mercury layer, due to the surface tension of the interface, the head of the thermistor is still surrounded by FC77 but the thermistor can already sense the signals from the mercury layer. Thus the temperature gradient and temperature fluctuation drop gradually, but are still larger than those in the pure conductive bulk of the mercury layer. We believe this region is not the boundary layer of the mercury layer as the Rayleigh number of the mercury layer is only 63, which is far below the onset Ra $= 1101$ for a fluid layer with one boundary slip

and the other boundary nonslip, and the rms does not have a peak. Instead this region should be the transitional region as a result of the deformed interface between mercury and FC77. The last region is the bulk region of the mercury layer, where the mean temperature increases linearly. The constant temperature gradient in the mercury layer indicates pure conduction inside, which is confirmed by the absence of peak in the rms temperature profile and very small temperature fluctuation.

Figure 2(c) shows the time series of temperatures at the four typical positions marked as A, B, C, and D, as shown in Fig. 2(a). Point A ($z_1 = 1$ mm) is outside the thermal boundary layer of the FC77 layer, and it can be found that the time trace of temperature shows a large number of positive spikes due to hot plumes released from the thermal boundary layer. Accordingly, the corresponding probability density function (PDF) is skewed toward higher temperature, as shown in Fig. 2(b). Point B ($z_1 = 0.2$ mm) is near the FC77-mercury interface and inside the thermal boundary layer of the FC77 layer, and small, mostly positive, but also some negative peaks on a more fluctuating baseline could be observed. The PDF of the temperature fluctuation is nearly Gaussian shaped except for the slightly longer left tail, as shown in Fig. 2(b), which is similar to that in the single-layer convection [48,50–52]. Point C ($z_1 = -0.1$ mm) is close to the mercury-FC77 interface and inside the mercury layer, the temperature fluctuation is still relatively strong due to the influence of the FC77 layer, but is much weaker than those at positions A and B. And its PDF also approximately conforms to Gaussian distribution. Point D ($z_1 = -2.4$ mm) is near the bottom plate and well in the mercury layer, it is found that the temperature seems to fluctuate randomly with very small fluctuations and the corresponding PDF remains in the Gaussian shape, as shown in Fig. 2(b). Plumes should dominate at point D if a convective flow exists like that in the FC77 layer; this is apparently not the case. Combining this with the mean temperature and rms temperature profile, we can conclude that no convection is taking place inside the mercury layer.

Similarly, we measured the temperature profile across the FC77-water interface, as shown in Fig. 3. In the bulk region of the FC77 layer, at position A, e.g., $z_2 = -1.5$ mm, the temperature trace shows lots of negative spikes due to the emission of the cold plumes as shown in Fig. 3(c), thus the corresponding PDF skews toward lower temperature. Inside the thermal boundary layer of the FC77 layer at position B ($z_2 = -0.3$ mm), one sees strong temperature fluctuations in both directions which is also corroborated by the peak in the rms temperature profile. As the distance to the top plate decreases, the temperature fluctuation gradually decreases and the PDFs at the positions C and D, e.g., $z_2 = 0.1, 1.3$ mm, are always close to a Gaussian distribution. Inside the water layer, the mean temperature decreases slowly and no peak in the rms temperature profiles is observed. It is seen that right after the thermistor crosses the interface (say, position C) the temperature gradient becomes smaller than that in the FC77 layer, but it is still larger than that in the bulk of the water layer where the temperature gradient becomes constant (say, position D). We believe that the relatively larger temperature gradient at position C (compared to position D) is induced by the fact that although the thermistor is already in the water layer, it is still surrounded by FC77, i.e., the local interface is deformed due to the surface tension and forming a bump pointing to the water side when the thermistor travels from the FC77 layer to the water layer. Similar to the argument for the mercury layer, we see no evidence of convection in the water layer for this case. One can see that at $z_2 = 2.9$ mm, the temperature is almost the same as at $z_2 = 2.5$ mm; this is due to the fact that the thermistor has already touched the bottom surface of the top plate around $z_2 = 2.5$ mm, which is observed by a traveling microscope. Note that this means a further increase of z_2 will result in the bending of the thermistor tip from the stem that connects the tip and the wires, while the tip itself will remain in touch with the top plate.

B. Determination of the temperature at the two interfaces of the FC77 layer

To calculate the Rayleigh number and the Nusselt number of the FC77 layer, we need to determine the temperature at the bottom and top interfaces of the FC77 layer. This can be done after the temperature profiles across the two interfaces have been measured. It is well known that inside a narrow region of the thermal boundary layer, the temperature varies almost linearly with
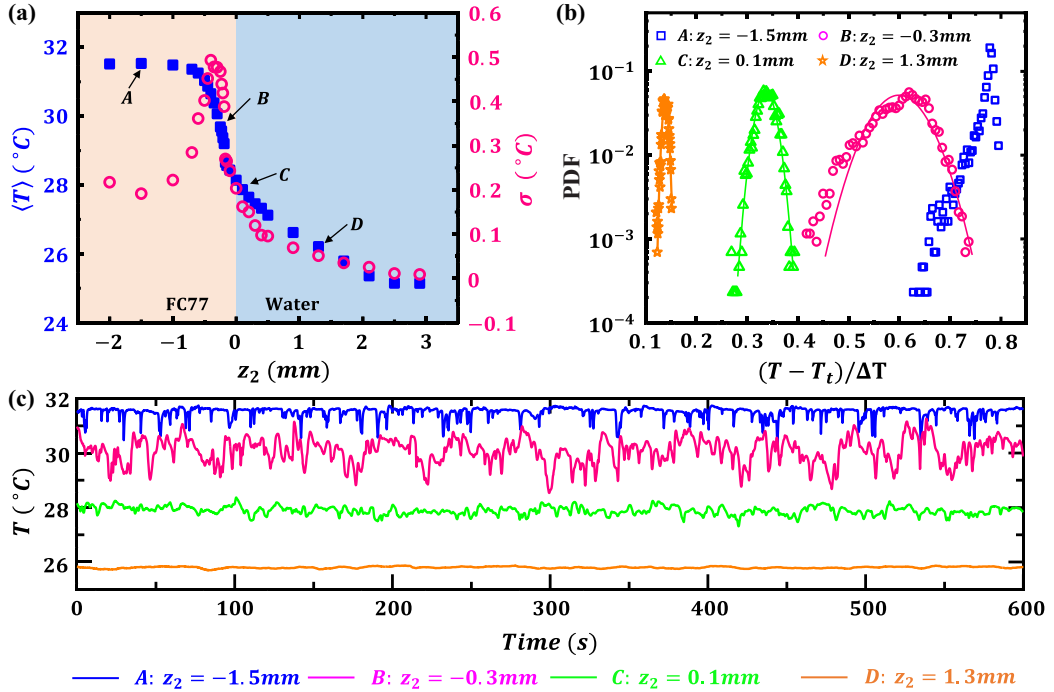
FIG. 3. (a) Mean temperature $\langle T \rangle$ and root-mean-square (rms) temperature σ profiles across the water and FC77 interface for Ra $= 3.85 \times 10^{10}$. Solid squares and open circles are $\langle T \rangle$ and σ. (c) The time series and (b) the PDF of temperatures measured at positions A, B, C, and D marked in (a). Please note that plotted in (b) is the PDF of $(T - T_t)/\Delta T$, not the temperature T itself, where T_t is the temperature of the top plate and ΔT is the temperature difference across the FC77 layer. The curves in (b) are the Gaussian distribution function fits to the data.

the distance from the boundary [48,53,54]. Such a situation can be also applied to the FC77 layer in the three-layer system, as shown in Fig. 4. In addition, as shown in Figs. 2 and 3, there is no peak in the rms temperature profiles in the thin mercury and water layers, which suggests there is no convective flow in the two thin layers. Thus, the mean temperature develops linearly in the mercury and water layers because heat is transported by conduction in both layers. Therefore, in the ideal case, one expects the interface to be the place where the linear region of the FC77 boundary layer intersects with the conductive mercury or water layer. As shown in Fig. 4(a), the intersection of the conductive mercury layer and the FC77 layer occurs at $z_1 = -0.035$ mm, which is very close to the interface determined by the traveling microscope. Similarly, in Fig. 4(b), the intersection of the FC77 and water layers is observed as $z_2 = -0.011$ mm, which is also close to the interface determined by the traveling microscope. Accordingly, the temperature at the intersection is regarded as the temperature at the interface. Based on the so determined temperatures at the interfaces, Nu and Ra can be calculated and their relationship is obtained. It should be noted that extrapolations had to be made to estimate the temperature difference across the FC77 layer, which could impact the reported scaling laws with the convective fluid boundaries. It also should be noted that unlike in the case of the canonical single-layer convection under the Boussinessq condition, the temperature at the top and bottom interfaces of the FC77 layer in the three-layer system is not symmetric with respect to the temperature at the center of the FC77 layer. For example, when Ra $= 3.85 \times 10^{10}$, the temperature at the top interface, center, and the bottom interface is 27.60 °C, 31.62 °C, and 36.03 °C, respectively. The temperature difference between the top interface and the center ΔT_t is 4.02 °C, while the temperature difference between the bottom interface and the center of the FC77
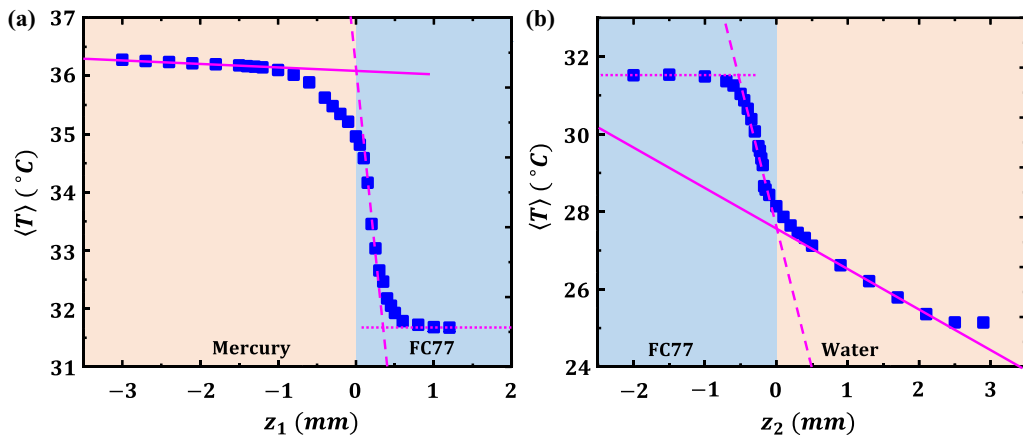
FIG. 4. Mean temperature profile across (a) the mercury-FC77 interface and (b) the FC77-water interface for 3.85×10^{10}. The solid lines are the linear fits to the temperature in (a) the mercury layer and (b) the water layers. The dashed lines and the dotted lines in (a) and (b) are the linear fits to the linear parts and the constant temperature parts in the lower and upper boundary regions of the FC77 layer, respectively. One can see that in (b) at $z_2 = 2.9$ mm, the temperature is almost the same as at $z_2 = 2.5$ mm. This is because the thermistor has already touched the bottom surface of the top plate around $z_2 = 2.5$ mm, which is observed by a traveling microscope. Note: This means a further increase of z_2 will result in bending of the thermistor tip from the stem that connects the tip and the wires, while the tip itself will remain in touch with the top plate.

layer ΔT_b is 4.39 °C. This asymmetry in the temperature drop is a result of the asymmetric thermal boundary layer thickness that will be discussed in Sec. III C.

C. Heat transfer

Once the temperatures at the top and bottom interfaces of the FC77 layer are determined, we are able to calculate Nu and Ra of the FC77 layer. Figure 5(a) shows the dependence of Nu on Ra of the FC77 layer in the three-layer system; it is found that Nu scales with Ra as $Nu = 0.119Ra^{0.31}$ in the low Ra range and as $Nu = 0.021Ra^{0.38}$ in the high Ra range, and the transition of the scaling exponent begins at Ra $\approx 2.52 \times 10^{10}$. For comparison, we also plot Nu for the canonical
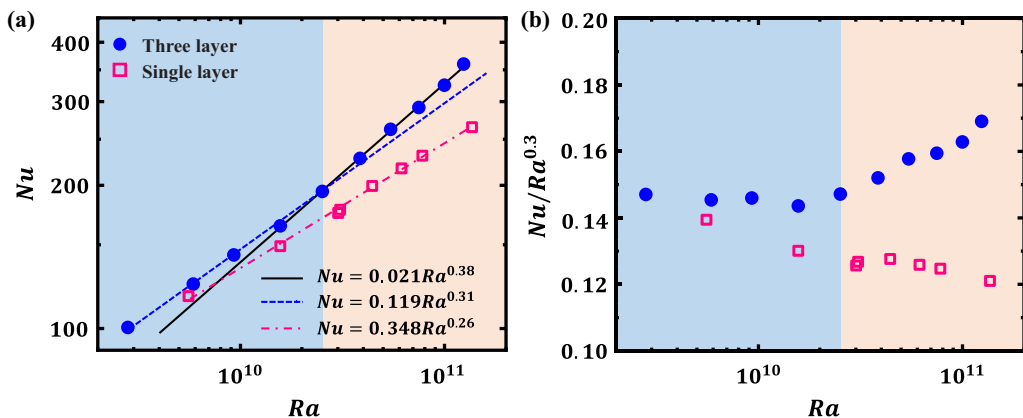

FIG. 5. (a) Nu as a function of Ra for the FC77 layer in the three-layer system and the single-layer system. (b) The same as in (a) with Nu is compensated by $Ra^{0.3}$.
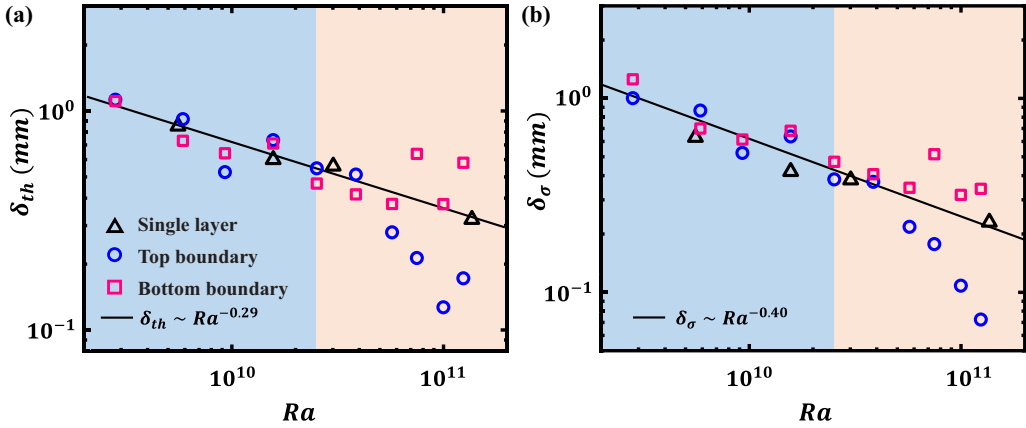
FIG. 6. Thickness of the top and bottom boundary layers of the FC77 layer (a) obtained from the mean temperature profile δ_{th} and (b) obtained from the rms temperature profile δ_σ as a function of Ra in the FC77 layer. The boundary layer thickness of the FC77 layer in the single-layer experiments is presented for comparison.

single-layer FC77 experiments conducted for the same range of Ra and at the same value of Pr [55]; the scaling between Nu and Ra can be well fitted by $Nu = 0.348Ra^{0.26}$ in the whole range of Ra under study, which is in agreement with the findings in the same Pr range [56]. Comparing the results from the three-layer and single-layer experiments, we can see that the existence of the liquid-liquid slippery boundary conditions at the top and bottom of the FC77 layer leads to a significant increase in the scaling exponent of heat transport, from 0.26 to 0.31 in the low Ra range and from 0.26 to 0.38 in the high Ra range. The great increase of the scaling exponent is better illustrated in the compensated plot of Nu versus Ra as shown in Fig. 5(b). The existence of the slippery boundary conditions also leads to a great enhancement of the heat transfer; for example, Nu is enhanced by about 26% at $Ra = 10^{11}$.

It is found that the scaling exponent of Nu versus Ra increases with Ra when the liquid-solid boundary condition is changed to the liquid-liquid slippery boundary condition. Thus, a natural question is what determines the increase of the scaling. It is known that the thermal boundary layer (TBL) thickness is related to Nu via the relationship $\delta_{th} = H/2Nu$ when the bottom and top TBLs are symmetric [56–60]. This is the case for thermal convection with nonslip boundary conditions. Hence, we further evaluate the TBL thickness of the FC77 layer near the bottom and top interfaces to explore the influence of the mercury and water layers. Generally, the TBL thickness is determined by two methods [50]. The first one is based on the linear slope of the mean temperature $\langle T \rangle$ profile near the interface, also referred to as the slope method. As shown in Fig. 4, the distance between the interface and the position where the extrapolation of the linear part of the mean temperature meets the horizontal line passing through the bulk temperature, is defined as the thickness of the TBL δ_{th}. The other one is based on the peak position of the rms temperature σ, as shown in Figs. 2(a) and 3(a), based on the assumption that the temperature fluctuation is strongest at the edge of the TBL. The thickness of the TBL δ_σ is defined as the distance between the interface and the peak position of the rms temperature. It has been extensively reported that the TBL thicknesses determined by the two methods share the same trend, but the mean temperature method yields a slightly smaller boundary layer thickness and a sharper scaling exponent between the thickness and Ra compared to those determined from the rms temperature method [48,50,61]. Figures 6(a) and 6(b) show the TBL thickness determined from the mean temperature profile and the rms temperature profile, respectively. It can be seen from the figure that the TBL thickness obtained from the two different methods gives very similar results; δ_{th} and δ_σ are not only close in trend but also very close in amplitude.

For comparison, the TBL thickness in the canonical single-layer system with FC77 is also shown in Fig. 6. It is found from the figure that in the mercury-FC77-water three-layer system the TBL thickness of the FC77 layer above the FC77-mercury interface (both δ_{th} and δ_σ) follows the similar trend as that in the case of the solid boundary condition in the single-layer system. However, the TBL thickness below the water-FC77 interface (both δ_{th} and δ_σ) does not always follow the similar trend of the solid boundary case; in particular, there is a transitional Ra, above which the TBL thickness (both δ_{th} and δ_σ) becomes smaller, and follows a steeper scaling slope. Because of the experimental difficulties, the data are rather scattered. To gauge the broad trend of TBL thickness on Ra, we make power-law fits to the data, which yields scaling exponent -0.29 (-0.40) for δ_{th} (δ_σ) before the transition (Ra $< 3.85 \times 10^{10}$), and -1.43 (-1.36) after the transition (Ra $> 3.85 \times 10^{10}$). The transitional Ra in the scaling of the TBL thickness on Ra is very close to that in the scaling of Nu on Ra (Ra $\approx 2.52 \times 10^{10}$ vs Ra $\approx 3.85 \times 10^{10}$). From the similar trend of TBL thickness dependence on Ra for the FC77-solid boundary condition in the single-layer system and the FC77-mercury boundary condition in the three-layer system, we can see that the FC77-mercury boundary is not so different from the FC77-solid boundary in terms of the TBL thickness.

The original objective of the current study is to achieve a slip (or a partially slip) boundary condition at both the top and the bottom interfaces. It seems that the slip (or partially slip) boundary condition is achieved at both interfaces, which is reflected by the increase of the Nu vs Ra scaling exponent (from 0.26 to 0.31 then 0.38) compared to the case with both solid boundary conditions at the top and the bottom. On the other hand, the level of slippery at the FC77-water interface and the FC77-mercury interface may be different, especially in the high Ra range, where the TBL becomes much thinner near the FC77-water interface compared with the solid boundary condition case. Thus, it is reasonable to assume that the FC77-water interface is more slippery. As we have achieved a more slippery top interface, we can conduct a hypothetical experiment where the bottom boundary condition (hypothetically achieved at the interface between FC77 and a certain "waterlike" fluid but with density higher than FC77) is the same as the top boundary condition (achieved at the FC77-water interface). We denote this as a "water-FC77-water" three-layer system.

In the calculation of the Rayleigh number Ra $= \alpha g H^3 \Delta T / (\nu \kappa)$ and the Nussult number Nu $= J/(\lambda \Delta T/H)$ of the FC77 layer, the temperature difference across the FC77 layer is ΔT. If we denote the temperature difference between the top interface and the middle height of the FC77 layer as ΔT_t, and similarly the temperature difference between the bottom interface and the middle height of the FC77 layer as ΔT_b, then $\Delta T = \Delta T_t + \Delta T_b$. As shown in previous studies, the mean temperature in the bulk region does not vary appreciably, thus ΔT_t and ΔT_b are also the temperature drops across the top and bottom boundary layers. In the hypothetical water-FC77-water three-layer system the temperature drop across the bottom boundary layer ΔT_b now should be the same as that across the top boundary layer ΔT_t, i.e., the temperature difference across the FC77 layer is $2\Delta T_t$. With this new temperature difference, $\Delta T = 2\Delta T_t$, we can calculate the new Ra and Nu for the FC77 layer in this hypothetical water-FC77-water three-layer system. Similarly, we can also calculate the new Ra and Nu for the FC77 layer in the hypothetical "mercury-FC77-mercury" three-layer system. In the calculation of Nu in the hypothetical experiments, we assume that the heating power is the same as that in the water-FC77-mercury system, as the mean temperature in the bulk region of the FC77 layer does not vary appreciably, or equivalently, Nu $\gg 1$ in the bulk region.

In Fig. 7 we plot Nu as a function of Ra for the FC77 layer in the hypothetical water-FC77-water and mercury-FC77-mercury systems. For comparison we also plot the data from the canonical single FC77 layer experiment, and from the water-FC77-mercury three-layer experiment. It is clear from Fig. 7(a) that the mercury-FC77-mercury data follows the scaling of Nu $= 0.113$Ra$^{0.31}$ in the entire Ra range. In contrast, the water-FC77-water data shows a clear transition, and the transitional Ra is the same as that in the water-FC77-mercury system. After the transition the water-FC77-water data can be well fitted by Nu $= 0.003$Ra$^{0.46}$. The Ra dependence of Nu for different boundary conditions and the transition in the scaling law are made more obvious in the compensated plot of Nu versus Ra, as shown in Fig. 7(b). Taking everything together, one sees that the slip boundary generated by the water layer is the key to the transition of the heat transport scaling law. To understand the
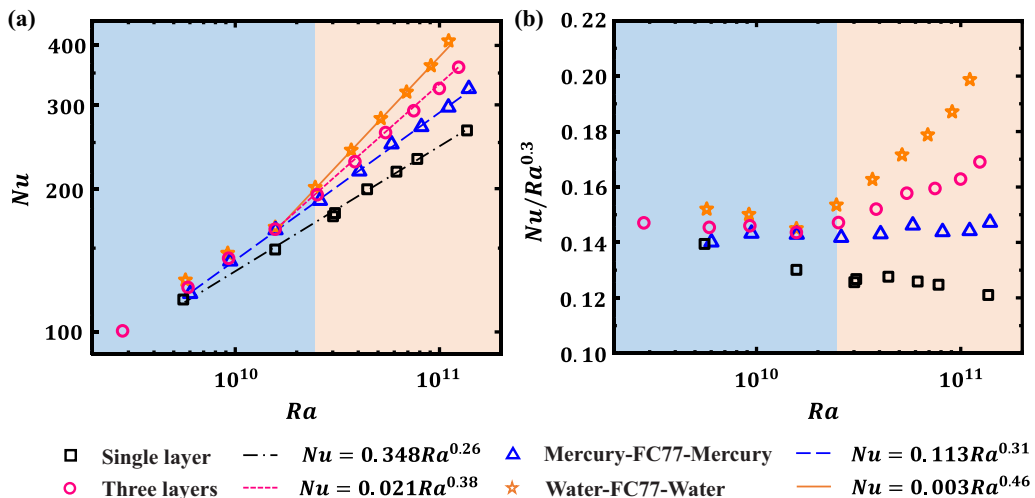
FIG. 7. (a) Nu obtained from a hypothetical system where a FC77 layer is sandwiched between two identical water layers (denoted by "water-FC77-water") or two identical mercury layers (denoted by "mercury-FC77-mercury"). (b) The corresponding compensated Nusselt number $Nu/Ra^{0.3}$ as a function of Ra. The circles and squares are respectively the three-layer and single layer results already shown in Fig. 5.

transition to the higher scaling exponent, we examine the flow states in the thin water layer as well as the thin mercury layer. The flow states of the two layers are determined by their respective Ra, which are shown in Table II. It is seen that the mercury layer always maintains a conduction state, as reflected by the fact that Ra is always lower than the critical Ra for the onset of convection for the mercury case ($Ra_c = 1101$). While for the water layer, the critical Ra for the onset of convection is 1101 for a configuration where one boundary condition is slip and the other is nonslip [62]. The Ra range in the current study crosses the critical Ra, thus the water layer gradually transitions from a conductive state to a convective state. From Table II one can see that $Ra_w = 1101$ corresponds to Ra (of the FC77 layer) being between 2.52×10^{10} and 3.85×10^{10}, which is almost the same as the transitional Ra for Nu vs Ra scaling and the transitional Ra for the scaling of the TBL thickness. Therefore it is clear that the transition to Nu scaling of $Ra^{0.46}$ and the transition of the TBL thickness are due to the transition of the state of the water layer from conduction to convection. We note that the value of Ra in the water layer, though above that for the onset of convection, is still considerably smaller than those for turbulent flows, so the FC77-water interface remains nearly flat and quiescent, and the temperature profile in the water layer is also largely linear as observed in our experiments. Thus, the convective motion in the thin water layer may be regarded as providing a boundary condition for the top FC77 layer that is viscously slippery and thermally with an enhanced effective thermal conductivity. The mercury layer also results in a significant transition of the scaling exponent (from 0.26 to 0.31), but is less significant compared to the water layer (from 0.26 to 0.46); and it also enhances heat transport compared to the canonical single-layer system. The results with the mercury-FC77-mercury system are consistent with previous experiments with a sheared thin mercury layer at the bottom of a thick layer of water [38,39].

TABLE II. The Rayleigh numbers of the water [Ra_W], FC77 [Ra_F] and mercury [Ra_{Hg}] layers in the current experiment. The onset Rayleigh number for convection with top (bottom) nonslip and bottom (top) slip boundary conditions is 1101, and it is independent of Pr [62].

Ra_W	11	86	377	826	1437	1845	2362	2669	2639
$Ra_F(\times 10^{10})$	0.588	0.929	1.57	2.52	3.85	5.44	7.48	9.98	12.4
Ra_{Hg}	17	21	28	41	63	91	123	155	218

IV. SUMMARY AND CONCLUSION

We have made an experimental investigation on the heat transport of a FC77 layer in the water-FC77-mercury three-layer turbulent convection system. Both the top and the bottom boundaries are now liquid-liquid slippery boundaries, instead of the liquid-solid nonslip boundary in the canonical single-layer Rayleigh-Bénard convection system. We measured the temperature profiles across the FC77-water and FC77-mercury interfaces. From the temperature profiles we determined the temperatures at the two interfaces, which enabled us to calculate Ra and Nu of the FC77 layer. The thickness of the top and bottom TBL of the FC77 layer are also determined from the measured temperature profiles. It is found that the measured Nu of the FC77 layer in the three-layer system is much larger than that of an identical single FC77 layer system but with solid top and bottom boundaries, indicating enhanced heat transfer under the slippery boundaries. In addition, the exponent of Nu vs Ra scaling also increases with the slippery boundary condition, i.e., $\mathrm{Nu} = 0.113\mathrm{Ra}^{0.31}$ for $\mathrm{Ra} \leqslant 2.52 \times 10^{10}$ and $\mathrm{Nu} = 0.021\mathrm{Ra}^{0.38}$ for $\mathrm{Ra} \geqslant 2.52 \times 10^{10}$. In comparison, for the canonical single FC77 layer with solid boundaries with the same Ra range and for the same value of Pr, we found $\mathrm{Nu} = 0.348\mathrm{Ra}^{0.26}$.

It is found that the thickness of the bottom (in contact with the mercury layer) TBL is almost the same as that in the single-layer system, whereas the thickness of the top TBL initially follows that in the canonical single-layer system, then changes to a steeper scaling with Ra when $\mathrm{Ra} > 3.85 \times 10^{10}$, which is very close to the transitional Ra for Nu vs Ra scaling. The different behavior of the top and bottom TBLs implies that the thin water layer and the thin mercury layer exert different boundary conditions for the FC77 layer. This prompted us to envision two hypothetical experiments wherein the top and the bottom boundary conditions are symmetric, denoted as water-FC77-water three-layer system and mercury-FC77-mercury three-layer system. In both systems the temperature drop across the bottom boundary layer ΔT_b would be the same as that across the top boundary layer ΔT_t. We find that in the hypothetical water-FC77-water three-layer system, with the increase of Ra, Nu vs Ra scaling transitions from $\mathrm{Nu} = 0.113\mathrm{Ra}^{0.31}$ to $\mathrm{Nu} = 0.003\mathrm{Ra}^{0.46}$ with the transitional Ra the same as identified for the real mercury-FC77-water system. Whereas for the mercury-FC77-mercury three-layer system, no transition in Nu vs Ra scaling is observed. Instead, in the entire Ra range, Nu scales with Ra with a single power law: $\mathrm{Nu} = 0.113\mathrm{Ra}^{0.31}$. A closer check of the evolution of Rayleigh numbers of the water layer, FC77 layer, and the mercury layer reveal that the transition of Nu vs Ra scaling in the real system as well as in the hypothetical water-FC77-water system can be attributed to the transition of the thin water layer from a conduction state to a convection state. It is therefore clear that the conduction to convection transition in the water layer is the key to the transition of the heat transport scaling law. The scaling exponent between Nu and Ra obtained in the hypothetical water-FC77-water three-layer system is very close to the one obtained in a previous simulation of turbulent RBC with both the thermal and the viscous boundary layers removed, which produces a Nu-Ra scaling exponent of 1/2 [63]. It should be noted that in the hypothetical water-FC77-water three-layer system, the viscous boundary layers might be "removed" or "partially removed" due to the slip or partially slip boundary conditions for the FC77 layer, while the thermal boundary layers are still there, only the top thermal boundary layer becomes thinner than that in the canonical single-layer system when Ra exceeds the transitional Ra. In the future, it would be highly desirable to determine quantitatively the properties of the two viscous boundary layers of the FC77 layer, which would require precision velocity field measurements across the top and bottom interfaces of the FC77 layer.

[1] G. Ahlers, S. Grossmann, and D. Lohse, Heat transfer and large scale dynamics in turbulent Rayleigh-Bénard convection, Rev. Mod. Phys. **81**, 503 (2009).

[2] D. Lohse and K. Q. Xia, Small-scale properties of turbulent Rayleigh-Bénard convection, Annu. Rev. Fluid Mech. **42**, 335 (2010).

[3] K. Q. Xia, S. D. Huang, Y. C. Xie, and L. Zhang, Tuning heat transport via coherent structure manipulation: Recent advances in thermal turbulence, Natl. Sci. Rev. **10**, nwad012 (2023).

[4] S. X. Guo, S. Q. Zhou, X. R. Cen, L. Qu, Y. Z. Lu, L. Sun, and X. D. Shang, The effect of cell tilting on turbulent thermal convection in a rectangular cell, J. Fluid Mech. **762**, 273 (2015).

[5] O. Shishkina and S. Horn, Thermal convection in inclined cylindrical containers, J. Fluid Mech. **790**, R3 (2016).

[6] A. Teimurazov and P. Frick, Thermal convection of liquid metal in a long inclined cylinder, Phys. Rev. Fluids **2**, 113501 (2017).

[7] L. Zwirner and O. Shishkina, Confined inclined thermal convection in low-Prandtl-number fluids, J. Fluid Mech. **850**, 984 (2018).

[8] R. Khalilov, I. Kolesnichenko, A. Pavlinov, A. Mamykin, A. Shestakov, and P. Frick, Thermal convection of liquid sodium in inclined cylinders, Phys. Rev. Fluids **3**, 043503 (2018).

[9] S. D. Huang, M. Kaczorowski, R. Ni, and K. Q. Xia, Confinement-induced heat-transport enhancement in turbulent thermal convection, Phys. Rev. Lett. **111**, 104501 (2013).

[10] S. D. Huang and K. Q. Xia, Effects of geometric confinement in quasi-2-D turbulent Rayleigh-Bénard convection, J. Fluid Mech. **794**, 639 (2016).

[11] Y. Bao, J. Chen, B. F. Liu, Z. S. She, J. Zhang, and Q. Zhou, Enhanced heat transport in partitioned thermal convection, J. Fluid Mech. **784**, R5 (2015).

[12] K. L. Chong, S. Wagner, M. Kaczorowski, O. Shishkina, and K. Q. Xia, Effect of Prandtl number on heat transport enhancement in Rayleigh-Bénard convection under geometrical confinement, Phys. Rev. Fluids **3**, 013501 (2018).

[13] L. Zhang and K. Q. Xia, Achieving heat transfer enhancement via manipulation of bulk flow structures in turbulent thermal convection, Phys. Rev. Fluids **8**, 023501 (2023).

[14] S. Wagner and O. Shishkina, Heat flux enhancement by regular surface roughness in turbulent thermal convection, J. Fluid Mech. **763**, 109 (2015).

[15] Y. C. Xie and K. Q. Xia, Turbulent thermal convection over rough plates with varying roughness geometries, J. Fluid Mech. **825**, 573 (2017).

[16] Y. Z. Zhang, C. Sun, Y. Bao, and Q. Zhou, How surface roughness reduces heat transport for small roughness heights in turbulent Rayleigh-Bénard convection, J. Fluid Mech. **836**, R2 (2018).

[17] J. L. Yang, Y. Z. Zhang, T. C. Jin, Y. H. Dong, B. F. Wang, and Q. Zhou, The-dependence of the critical roughness height in two-dimensional turbulent Rayleigh-Bénard convection, J. Fluid Mech. **911**, A52 (2021).

[18] M. Belkadi, A. Sergent, Y. Fraigneau, and B. Podvin, On the role of roughness valleys in turbulent Rayleigh-Bénard convection, J. Fluid Mech. **923**, A6 (2021).

[19] M. Sharma, K. Chand, and A. K. De, Investigation of flow dynamics and heat transfer mechanism in turbulent Rayleigh-Bénard convection over multi-scale rough surfaces, J. Fluid Mech. **941**, A20 (2022).

[20] J. Q. Zhong, D. Funfschilling, and G. Ahlers, Enhanced heat transport by turbulent two-phase Rayleigh-Bénard convection, Phys. Rev. Lett. **102**, 124501 (2009).

[21] R. Lakkaraju, R. J. A. M. Stevens, P. Oresta, R. Verzicco, D. Lohse, and A. Prosperetti, Heat transport in bubbling turbulent convection, Proc. Natl. Acad. Sci. USA **110**, 9237 (2013).

[22] Z. Q. Wang, V. Mathai, and C. Sun, Self-sustained biphasic catalytic particle turbulence, Nat. Commun. **10**, 3333 (2019).

[23] S. Y. Hu, K. Z. Wang, L. B. Jia, J. Q. Zhong, and J. Zhang, Enhanced heat transport in thermal convection with suspensions of rod-like expandable particles, J. Fluid Mech. **928**, R1 (2021).

[24] A. Blass, X. J. Zhu, R. Verzicco, D. Lohse, and R. J. A. M. Stevens, Flow organization and heat transfer in turbulent wall sheared thermal convection, J. Fluid Mech. **897**, A22 (2020).

[25] A. Blass, P. Tabak, R. Verzicco, R. J. A. M. Stevens, and D. Lohse, The effect of Prandtl number on turbulent sheared thermal convection, J. Fluid Mech. **910**, A37 (2021).

[26] T. C. Jin, J. Z. Wu, Y. Z. Zhang, Y. L. Liu, and Q. Zhou, Shear-induced modulation on thermal convection over rough plates, J. Fluid Mech. **936**, A28 (2022).

[27] A. Xu, B. R. Xu, and H. D. Xi, Wall-sheared thermal convection: Heat transfer enhancement and turbulence relaminarization, J. Fluid Mech. **960**, A2 (2023).

[28] J. Mac Huang and J. Zhang, Rayleigh–Bénard thermal convection perturbed by a horizontal heat flux, J. Fluid Mech. **954**, R2 (2023).

[29] B. F. Wang, Q. Zhou, and C. Sun, Vibration-induced boundary-layer destabilization achieves massive heat-transport enhancement, Sci. Adv. **6**, eaaz8239 (2020).

[30] J. Z. Wu, B. F. Wang, K. L. Chong, Y. H. Dong, C. Sun, and Q. Zhou, Vibration-induced 'anti-gravity' tames thermal turbulence at high Rayleigh numbers, J. Fluid Mech. **951**, A13 (2022).

[31] Z. L. Huang, X. L. Guo, J. Z. Wu, B. F. Wang, K. L. Chong, and Q. Zhou, Rayleigh-number dependence of the critical vibration frequency in vibrating thermal turbulence, Phys. Rev. Fluids **8**, 113501 (2023).

[32] M. J. Huang, Y. Wang, Y. Bao, and X. Z. He, Heat transport and temperature boundary-layer profiles in closed turbulent Rayleigh-Bénard convection with slippery conducting surfaces, J. Fluid Mech. **943**, A2 (2022).

[33] L. Cserepes and M. Rabinowicz, Gravity and convection in a two-layer mantle, Earth Planet. Sci. Lett. **76**, 193 (1985).

[34] S. Rasenat, F. H. Busse, and I. Rehberg, A theoretical and experimental study of double-layer convection, J. Fluid Mech. **199**, 519 (1989).

[35] A. Prakash and J. N. Koster, Steady Rayleigh-Bénard convection in a two-layer system of immiscible liquids, J. Heat Transfer **118**, 366 (1996).

[36] A. Prakash, K. Yasuda, K. Kuwahara, and T. Doi, Flow coupling mechanisms in two-layer Rayleigh-Bénard convection, Exp. Fluids **23**, 252 (1997).

[37] A. Davaille, Simultaneous generation of hotspots and superswells by convection in a heterogeneous planetary mantle, Nature (London) **402**, 756 (1999).

[38] T. H. Solomon and J. P. Gollub, Sheared boundary layers in turbulent Rayleigh-Bénard convection, Phys. Rev. Lett. **64**, 2382 (1990).

[39] T. H. Solomon and J. P. Gollub, Thermal boundary layers and heat flux in turbulent convection: The role of recirculating flows, Phys. Rev. A **43**, 6683 (1991).

[40] Y. C. Xie and K. Q. Xia, Dynamics and flow coupling in two-layer turbulent thermal convection, J. Fluid Mech. **728**, R1 (2013).

[41] M. Yoshida and Y. Hamano, Numerical studies on the dynamics of two-layer Rayleigh-Bénard convection with an infinite Prandtl number and large viscosity contrasts, Phys. Fluids **28**, 116601 (2016).

[42] M. Yoshida, H. Iwamori, Y. Hamano, and D. Suetsugu, Heat transport and coupling modes in Rayleigh-Bénard convection occurring between two layers with largely different viscosities, Phys. Fluids **29**, 096602 (2017).

[43] D. Noto, Y. Tasaka, and Y. Murai, Coupling structures of two-layer natural convection in a cylindrical vessel investigated by simultaneous two-layer visualization, Exp. Therm. Fluid Sci. **127**, 110394 (2021).

[44] H. R. Liu, K. L. Chong, Q. Wang, C. S. Ng, R. Verzicco, and D. Lohse, Two-layer thermally driven turbulence: Mechanisms for interface breakup, J. Fluid Mech. **913**, A9 (2021).

[45] H. R. Liu, K. L. Chong, R. Yang, R. Verzicco, and D. Lohse, Heat transfer in turbulent Rayleigh-Bénard convection through two immiscible fluid layers, J. Fluid Mech. **938**, A31 (2022).

[46] H. L. Huang, W. Xu, Y. Wang, X. P. Wang, X. Z. He, and P. Tong, Fluctuation-induced slip of thermal boundary layers at a stable liquid-liquid interface, J. Fluid Mech. **951**, A10 (2022).

[47] M. Wang, X. Y. Chen, W. Wang, and P. Wei, Heat transport and flow structure in thermal convection with two liquid layers, J. Fluid Mech. **978**, A4 (2024).

[48] S. L. Lui and K. Q. Xia, Spatial structure of the thermal boundary layer in turbulent convection, Phys. Rev. E **57**, 5494 (1998).

[49] S. Q. Zhou and K. Q. Xia, Spatially correlated temperature fluctuations in turbulent convection, Phys. Rev. E **63**, 046308 (2001).

[50] A. Belmonte, A. Tilgner, and A. Libchaber, Temperature and velocity boundary layers in turbulent convection, Phys. Rev. E **50**, 269 (1994).

[51] C. Sun, Y. H. Cheung, and K. Q. Xia, Experimental studies of the viscous boundary layer properties in turbulent Rayleigh-Bénard convection, J. Fluid Mech. **605**, 79 (2008).

[52] Q. Zhou and K. Q. Xia, Thermal boundary layer structure in turbulent Rayleigh–Bénard convection in a rectangular cell, J. Fluid Mech. **721**, 199 (2013).

[53] A. Belmonte, A. Tilgner, and A. Libchaber, Boundary layer length scales in thermal turbulence, Phys. Rev. Lett. **70**, 4067 (1993).

[54] Q. Zhou, R. J. A. M. Stevens, K. Sugiyama, S. Grossmann, D. Lohse, and K. Q. Xia, Prandtl–Blasius temperature and velocity boundary-layer profiles in turbulent Rayleigh–Bénard convection, J. Fluid Mech. **664**, 297 (2010).

[55] C. Qiu, Heat transfer measurement of multilayer immiscible fluid in turbulent thermal convection, Master's thesis, The Chinese University of Hong Kong, 2010.

[56] S. Grossmann and D. Lohse, Scaling in thermal convection: A unifying theory, J. Fluid Mech. **407**, 27 (2000).

[57] S. Grossmann and D. Lohse, Thermal convection for large Prandtl numbers, Phys. Rev. Lett. **86**, 3316 (2001).

[58] S. Grossmann and D. Lohse, Prandtl and Rayleigh number dependence of the Reynolds number in turbulent thermal convection, Phys. Rev. E **66**, 016305 (2002).

[59] S. Grossmann and D. Lohse, Fluctuations in turbulent Rayleigh-Bénard convection: The role of plumes, Phys. Fluids **16**, 4462 (2004).

[60] R. J. A. M. Stevens, E. P. van der Poel, S. Grossmann, and D. Lohse, The unifying theory of scaling in thermal convection: The updated prefactors, J. Fluid Mech. **730**, 295 (2013).

[61] R. du Puits, C. Resagk, A. Tilgner, F. H. Busse, and A. Thess, Structure of thermal boundary layers in turbulent Rayleigh-Bénard convection, J. Fluid Mech. **572**, 231 (2007).

[62] S. Chandrasekhar, *Hydrodynamic and Hydromagnetic Stability* (Courier Corporation, North Chelmsford, MA, 2013).

[63] D. Lohse and F. Toschi, Ultimate state of thermal convection, Phys. Rev. Lett. **90**, 034502 (2003).